A fully automated optical microscope for analysis of particle tracks in solids

M. Dolleiser, S.R. Hashemi-Nezhad *

Department of High Energy Physics, School of Physics, A28, University of Sydney, Sydney, NSW 2006, Australia

Abstract

A fully automatic optical microscope (FAOM) for on-line analysis of micro-objects is described. The system has many capabilities, such as autofocusing, autocounting, autoscanning, producing optical images corresponding to different depths in the sample, contour and edge finding, etc. The autofocusing can be achieved with more than one method. The system can be used for analysis and counting (high-density) micro-objects, such as particle tracks in plastic detectors. The processing speed of the system is adequate and it can be used in analysis of macro samples. The software of the FAOM is written in C++ and runs under Microsoft Windows operating systems.
© 2002 Elsevier Science B.V. All rights reserved.

Keywords: Automatic scanner; Optical microscope; Nuclear tracks

1. Introduction

There are several types of semi-automatic and automatic optical microscope systems with different capabilities that are used for analysis of particle tracks in solids (see e.g. [1–5]). Most of these systems are designed and built for a specific application and not all the details of their hardware and software are available. The commercially presented systems usually are too expensive and therefore are not affordable by all laboratories. Moreover in most cases these systems are rigidly set to perform certain functions and hence cannot be easily customised to the needs of the interested laboratories.

In an earlier publication [5] we have given the description of a computer controlled optical microscope (CCOM). CCOM is a low cost semi-automatic optical microscope system, which is capable of producing consecutive optical micro-images of transparent micro-objects, each image corresponding to a different depth in the sample. We refer to this process as optical slicing. CCOM also is used for counting and analysis of charged particle tracks in solid-state nuclear track detectors.

In this paper we describe a new fully automated optical microscope (FAOM). FAOM is a flexible system that can perform all the capabilities of the CCOM in a much improved manner plus extra functions such as capability of counting high-density tracks or similar objects in a given *micro/*

* Corresponding author. Tel.: +61-2-9351-5964; fax: +61-2-9351-7727.

E-mail address: reza@physics.usyd.edu.au (S.R. Hashemi-Nezhad).

macroscopic sample. All details of the hardware and software of the FAOM are described in details and in a manner that it can be built and implemented by the interested laboratories.

FAOM has more advanced and user-friendly software than CCOM, which works under Windows operating systems. Although in most cases proton and alpha tracks in CR39 and LR-115 plastic detectors were used to test FAOM and optimise its performance, system is a general purpose FAOM and may be used to study objects other than nuclear tracks.

2. Hardware

Fig. 1 shows a general view of the FAOM system. A detailed description of the hardware used in the system is given below.

2.1. Microscope

The microscope used in the FAOM is an old type manufactured by Cook, Troughton & Simms Ltd., York, England. To accommodate this microscope in the automatic system, we made a few changes and improvements:

- Replacement of the old 25 mm × 25 mm manually moving stage with a 102 mm × 102 mm motorised stage.
- Attachment of a stepper motor to the fine vertical movement knob.
- Mounting of end switches to the fine vertical movement mechanism.
- Adding a semiconductor power regulator to the illumination system.
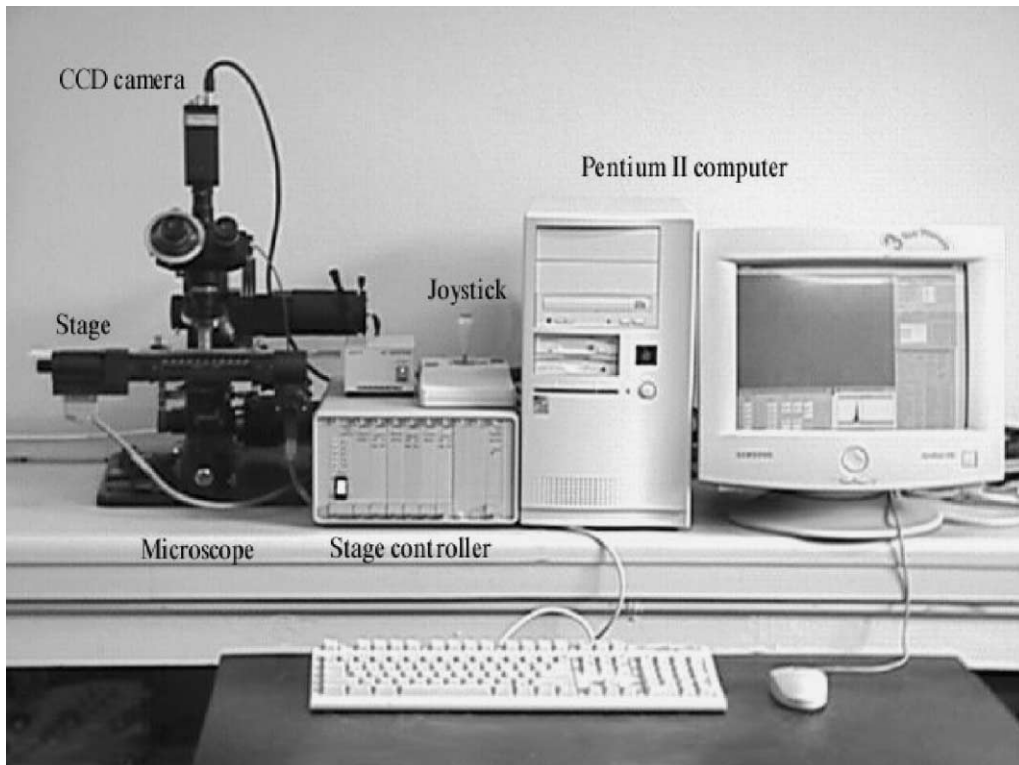- Attachment of a video camera in the place of the photographic camera.

Fig. 1. General view of the FAOM system.

2.2. Stage

The original stage was replaced with a BioPrecision Stage, manufactured by Ludl Electronic Products (LEP). Technical specifications of the stage are

- Part number – 99S001.
- Maximum travel – 102 mm × 102 mm.
- Resolution – 0.1 μm @ 30 mm/s speed.
- Repeatability – 0.75 μm.
- Full travel accuracy – 5 μm.

2.3. Stage controller

We used a LEP Modular Automation Controller MAC2000. The controller has nine slots available for different modules. In our case we used a configuration with three MDMSP (motor driver), three MCMSE (motor control) and one RS232INT modules. Two slots are left for possible future upgrades of the system. The stage controller is connected to a Pentium II based PC computer via the serial port and also can be controlled manually by a dedicated joystick.

There are two communication formats available:

- High-level format, which uses commands represented by human readable ASCII strings.
- Low-level format, where commands are in the binary form.

We used the low-level communication format, which we found more convenient to implement in the software.

2.4. Video camera

The video camera attached to the microscope is a monochrome charge coupled device (CCD) type C3077 manufactured by Hamamatsu. Some technical specifications of the camera are as follows:

- H/V resolution – 739(H)/575(V) picture elements.
- Signal system – CCIR.
- Horizontal scanning frequency – 15625 Hz.

- Vertical scanning frequency – 50 Hz.
- Sync system – 2:1 Interlace (625 lines, 50 Hz).
- CCD cell size – 11 μm × 11 μm.
- Weight – 190 g.
- Dimensions – 44 mm × 29 mm × 107 mm.
- Signal/noise – 50 dB (∼1 bit per byte).

2.5. Computer

The computer we use is a Pentium II, 350 MHz with 64 MB of RAM, running Microsoft Windows ME, although Windows 9× versions also can be used.

2.6. Frame grabber

To capture the camera output we use a cost effective CPI board: buz™ manufactured by iomega®. It is a combination of Ultra SCSII interface and video input, capture and output.

Technical specifications of the frame grabber are

- Resolution – up to 768 × 576 at 25 frames per second.
- Video in/out – composite and S-video.

These parameters fit very well to our video camera.

3. Software

To control FAOM hardware and to perform certain operations on the captured images we wrote the "Scanner.exe" programme. We used Microsoft Visual C++ version 6 to develop the application. The software is and will continue to be under development because of the new tasks that FAOM can perform in the future. Fig. 2 shows an image of the screen illustrating some features of the software. The current version of the source codes is available on the internet at: http://www.physics. usyd.edu.au/~marek/scanner/scanner.zip.

3.1. Features of the software

- Full control and monitoring position of the stage and focus adjustment.
- Tagging the positions of the stage to allow fast reviewing of the interesting parts of the sample.
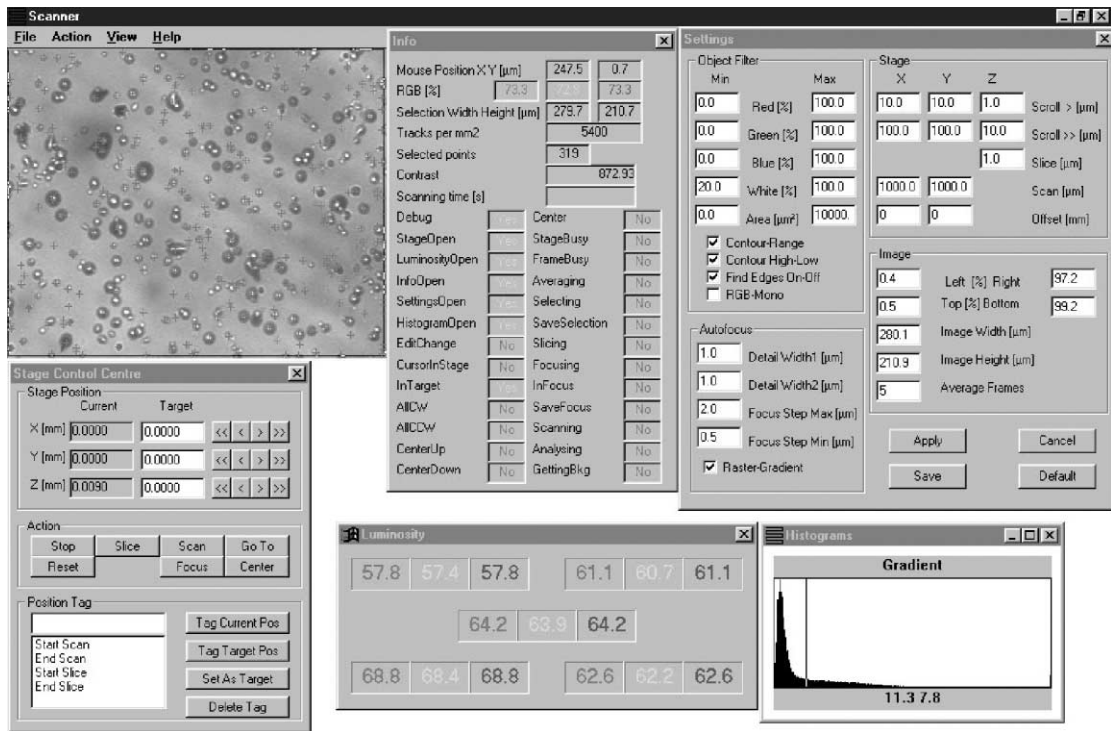
Fig. 2. Snapshot of the FAOM software screen.

- Automatic focusing.
- Video camera adjustment.
- Viewing the microscopic image on the monitor.
- Monitoring average and local (under cursor) image luminosity.
- Displaying image histograms.
- Selecting a portion of the image.
- Marking chosen points on the image.
- Differentiating the image (finding edges).
- Saving a selected part of the image to the bitmap file.
- Automatic scanning of user defined rectangle on the microscopic sample.
- Saving a series of images corresponding to different depths in the sample (optical slicing).
- Producing focus calibration file.
- Producing threshold calibration file.

3.2. Automatic focusing

Because of the variation of the focal plane from one field of view to another during scanning, au-

tomatic focusing is a very important function of the software. Object recognition and counting are extremely sensitive to the focus adjustment. In order to find the correct focal plane, the obvious method is to define a variable whose value depends on the contrast of the image. The actual focal plane at a given position on the sample can be found by maximising this variable. The question is how to define the contrast of the picture? There is not an universal definition for image contrast. The best is the one, which does the job with good accuracy and in the shortest time. We considered two methods: *gradient* method and *raster* method.

3.2.1. Gradient method

One can calculate the gradient of a picture using any of the many available differentiating matrix operators (Sobel's, cubic, etc.). Contrast is calculated as the sum of the gradient absolute values (or squares) over the chosen region of the picture. This method looks promising because it is fast and can have adjustable dimensions and elements of the

matrix operator can be fitted to a big variety of microscopic images. We built this method in the programme as an alternative to the raster method, which will be explained later in this paper. The user defines the parameter w (in μm) by means of "Detail width 1" in the "Settings" dialogue box of the programme. Differentiating matrices dX and dY of dimensions $(2w + 1)$ by $(2w + 1)$ are calculated as follows:

if
row $\neq w \wedge$ column $\neq w$
then

$$dX_{\text{row, column}} = \frac{\text{row} - w}{(\text{row} - w)^2 + (\text{column} - w)^2}$$

$$dY_{\text{row, column}} = \frac{\text{column} - w}{(\text{row} - w)^2 + (\text{column} - w)^2}$$

else

$$dX_{\text{row, column}} = dY_{\text{row, column}} = 0.$$

Matrices are indexed from 0, for compatibility with the C++ programming language.

The luminosity gradient at a point (x, y) with the colour index c is calculated from the formulae

$$\text{grad}_x(x, y, c) = \sum_{\text{row}=0}^{2w+1} \sum_{\text{column}=0}^{2w+1} dX_{\text{row, column}}$$
$$\times L(x + \text{column} - w, y + \text{row} - w, c),$$

$$\text{grad}_y(x, y, c) = \sum_{\text{row}=0}^{2w+1} \sum_{\text{column}=0}^{2w+1} dY_{\text{row, column}}$$
$$\times L(x + \text{column} - w, y + \text{row} - w, c),$$

$$\text{grad}(x, y, c)^2 = \text{grad}_x(x, y, c)^2 + \text{grad}_y(x, y, c)^2.$$

The contrast is then calculated from the formula

$$\text{contrast} = \sqrt{\sum_{c=0}^{c_{\max}} \sum_{y=y_{\min}}^{y_{\max}} \sum_{x=x_{\min}}^{x_{\max}} \text{grad}(x, y, c)^2},$$

where

- $c_{\max} = 0$ for a monochromatic image and $c_{\max} = 2$ for a colour (RGB) image,
- x and y are horizontal and vertical co-ordinates of the picture's pixel,

- $x_{\min}$, $y_{\min}$, $x_{\max}$ and $y_{\max}$ are co-ordinates of the corners of the bounding rectangle of the picture part chosen for autofocusing.
- $L(x, y, c)$ is the luminosity of the image's pixel at position (x, y) for colour c.

3.2.2. Raster method

In the raster method the contrast is calculated by the following formula using the vertical raster columns:

$$\text{contrast} = \sqrt{\sum_{c=0}^{c_{\max}} \sum_{y=y_{\min}}^{y_{\max}} \left(\sum_{x=x_{\min}}^{x_{\max}} C(x) L(x, y, c) \right)^2}.$$

The definition of the parameters in the above equation is the same as those given for the gradient method. $x_{\min}$, $y_{\min}$, $x_{\max}$ and $y_{\max}$ can be set arbitrarily but $x_{\max} - x_{\min}$ must be a multiple of the $w1 + w2$. $w1$ and $w2$ are calculated from Detail width 1 and Detail width 2 defined by the user in the Settings dialogue box.

$C(x)$ is defined as follows:

if $x \bmod (w1 + w2) < w1$

then $\quad C(x) = \frac{1}{w1} \quad$ else $\quad C(x) = \frac{-1}{w2}.$

This method of calculating the contrast uses only a raster in x-direction and is very fast.

3.3. Experimental tests of automatic focusing

We examined the gradient and raster methods experimentally, using CR39 plastic track detectors. The plastic detector contained proton recoil tracks that were induced by energetic neutrons with a wide energy range. The sample was etched for 6 h in 6N NaOH at 70 °C. Typical curves showing the variation of the contrast with depth in the sample are illustrated in Fig. 3 for the raster and gradient methods. To obtain the results shown in Fig. 3, we placed the sample under the microscope and the Z position (vertical movement) was adjusted manually to obtain the best possible focus by means of our subjective impression. Then we moved the objective lens down to acquire a blurred image. This position was tagged as $Z = 0$ μm. Then FAOM, starting from $Z = 0$, moved the objective

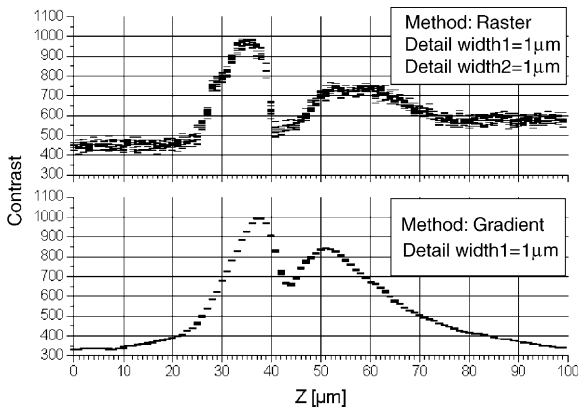Fig. 3. Contrast calculated by raster and gradient methods, as a function of Z position.

lens up in 100 steps of $dZ = 1$ μm. At every step the contrast was calculated using both methods. For every Z position 10 different frames were captured and contrast values were calculated. We used the same field of view and settings for both methods. As can be seen from Fig. 3, both methods give similar results with characteristics of two local maxima and one local minimum value. The gradient method produces a much smaller error and better-defined peaks than the raster method. The gradient method was only 30% slower than the raster method. Using bigger values for Detail width 1 slows down the gradient method without giving any significant improvement but does not change the raster method timing. Averaging of frames results in smaller errors in both methods.

Fig. 4 shows images that were captured at Z values corresponding to maxima and minimum in Fig. 3 (i.e. $Z = 37$, 44 and 51 μm). A simplified explanation of how these images are formed is shown in Fig. 5, using geometrical optics. Fig. 5(a) illustrates only the light rays that pass through the CR39 detector, the upper surface of which contains an etched track. For illumination of the specimen we use the Köhler method via a condenser of which the top lens has been removed and the aperture diaphragm was 50% closed. Thus the angle of the light cone reaching the specimen was small. The nearly parallel flux of light illuminating the specimen is refracted on the CR39–air interface and after passing through the microscope's $20\times$ objective lens (not shown in the drawing) reaches to the CCD camera. For clarity of the figure we do not show the illuminator light rays with angles different than $0°$ to the microscope's axis.

In Fig. 5(b) we have removed the light rays moving from the illuminator to the CR39–air interface and replaced them with the extended refracted rays. From Fig. 5(b) it can be seen that, if camera focus is set at the depth $Z = 37$ μm the observed track image has a bright spot in the centre surrounded by a dark ring. At the depth $Z = 44$ μm the track image is a disk, slightly darker than the background and at $Z = 51$ μm the track image is a dark disk surrounded by a bright ring. The image of the track at a certain depth depends on the track's shape and dimensions. The track
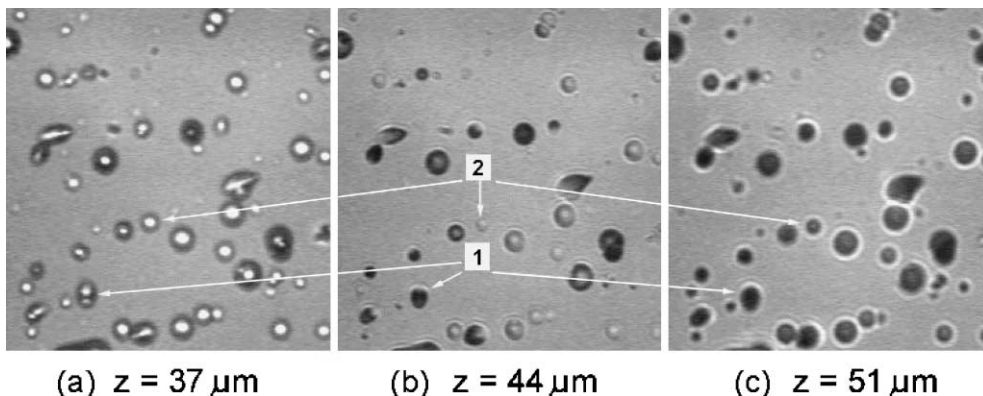

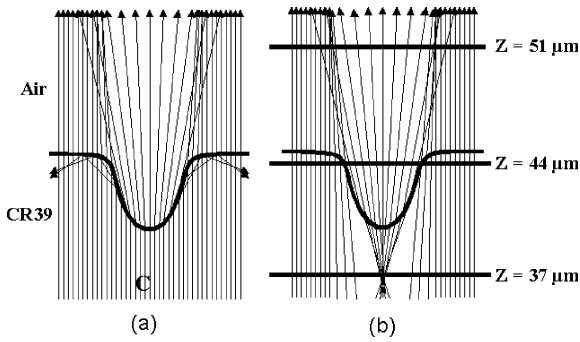Fig. 4. Track images at three characteristic Z positions.

Fig. 5. Simple geometrical explanation of the track images at different Z positions.

marked "2" in Fig. 4 is a good experimental illustration of the dependence of image shape on the position of the focal plane as shown in Fig. 5. Although the image corresponding to $Z = 44$ μm appears to be the "in focus" track image, for track counting purposes the best solution is to set the focus to that corresponding to $Z = 37$ μm in Fig. 4. This setting gives a good resolution for partially overlapped tracks, as illustrated by the track marked "1" in Fig. 4. Recognition of the partially overlapped tracks makes FAOM capable counting samples with high density of tracks.

3.4. Differentiating the image

To make the image less dependent on the specimen illumination, the user can choose the option "Find Edges" in the Settings dialogue box. If this option is enabled, a new image is produced from the analysed image using the formula

$$L_{new}(x, y, c) = \sqrt{grad(x, y, c)^2},$$

where

- $L_{new}(x, y, c)$ is the luminosity of the new image at position (x, y) for colour c,
- $grad(x, y, c)^2$ is calculated as described in the gradient method (Section 3.2.1).

3.5. Object counting

One of the main usages of the current version of FAOM is track density measurement in plastic de-

tectors. Tracks are defined by the threshold levels, which can be separately adjusted for each of the RGB colours or white if used with a monochromatic image. The user can adjust those parameters in "Red", "Green", "Blue" or "White" by entering "Min" and "Max" in the corresponding edit boxes. If the "Contour-Range" check box in the Settings dialogue box is checked, then the programme uses just the "Min" values for a given colour as the threshold. The recognition of the tracks starts with production of the image containing objects from the original or differentiated image. There are two options for the user to choose from: "High Contour" or "Low Contour". If the High Contour is chosen the points of the objects are defined as follows:

if

$$(L(x, y, c) \geqslant T_{min}(c)) \wedge \underset{\tilde{x}, \tilde{y}}{\exists}((|\tilde{x} - x| \leqslant 1)$$

$$\wedge (|\tilde{y} - y|) \leqslant 1) \wedge (L(\tilde{x}, \tilde{y}, c) < T_{min}(c))$$

then

$$L_{obj}(x, y, c) = 1$$

else

$$L_{obj}(x, y, c) = 0,$$

where

- $L(x, y, c)$ is the brightness of the analysed image at point (x, y) for given colour c,
- $T_{min}(c)$ is the threshold level for colour c as defined in the corresponding Min edit box,
- $L_{obj}(x, y, c)$ is the brightness of the object image at point (x, y) for given colour c.

If the Low Contour is chosen, object points are defined similarly,

if

$$(L(x, y, c) \leqslant T_{min}(c)) \wedge \underset{\tilde{x}, \tilde{y}}{\exists}((|\tilde{x} - x| \leqslant 1)$$

$$\wedge (|\tilde{y} - y|) \leqslant 1) \wedge (L(\tilde{x}, \tilde{y}, c) > T_{min}(c))$$

then

$$L_{obj}(x, y, c) = 1$$

else

$$L_{obj}(x, y, c) = 0.$$

If the Contour-Range check box in the Settings dialogue box is not checked, the object image points are defined as follows:

if

$$(L(x, y, c) \geqslant T_{\min}(c)) \wedge (L(\tilde{x}, \tilde{y}, c) \leqslant T_{\max}(c))$$

then

$$L_{\mathrm{obj}}(x, y, c) = 1$$

else

$$L_{\mathrm{obj}}(x, y, c) = 0.$$

$T_{\max}(c)$ is the upper limit for colour c defined in the corresponding Max edit box.

After the object image is created, the programme divides the whole picture into separated objects containing interconnected points with a brightness value of 1. The list of those objects with attributes like colour and a bounding rectangle is then filtered to remove objects that are too small or too big (by means of ''Area Min'' and ''Area Max'' parameters defined by the user). Also objects containing other objects inside them are removed from the list. This prevents double counting of the tracks that produce internal and external contours. The number of tracks left after this operation becomes the track counting result.

3.5.1. FAOM counting accuracy

Comparison of the performance of FAOM with other optical scanning systems is possible only by an inter-laboratory assessment, in which the same sample(s) is examined with different systems. This has not done by us at this stage. However the most obvious way of testing the performance of our system and its counting accuracy is to compare FAOM counts with those obtained by traditional manual counting of the tracks on the monitor screen.

In Fig. 6 image of a field of view corresponding to (mainly) alpha-tracks in LR-115 cellulose nitrate detector (Fig. 6(a)) is shown. Fig. 6(b) shows the tracks that are recognised by FAOM and are counted. The software of the FAOM places a red cross over the track when it was recognised as a track on the basis of the conditions chosen in the Settings' of the software (the red cross will not be visible for all tracks in a greyscale printout). Due to the relatively high track density in the field of view shown in Fig. 6, and presence of rather large number of overlapped tracks, in the Settings dialogue box of the FAOM Find Edges option was selected to increase the track resolution.

By comparing Fig. 6(a) and (b) one can see that all of the tracks are recognised and counted properly, i.e. all of the tracks are marked and overlapped tracks are recognised and counted as
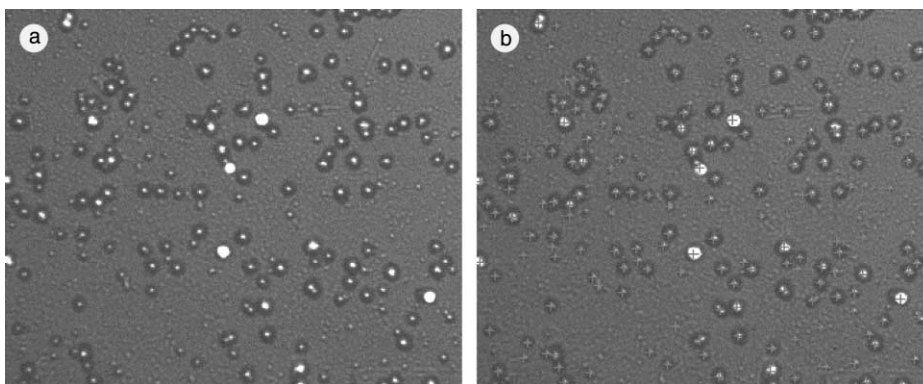

Fig. 6. (a) Image of a field of view corresponding to (mainly) alpha-tracks in LR-115 cellulose nitrate detector. (b) Tracks that are recognised by FAOM and are counted. The software of the FAOM places a red cross over the track when it was recognised as a track on the basis of the conditions chosen in the Settings dialogue box of the software (the red cross will not be visible for all tracks in a greyscale printout). Due to the relatively high track density in the field of view and presence of relatively large number of overlapped tracks, in the Settings dialogue box of the FAOM Find Edges option was selected to increase track resolution.

individual objects. The track density in the image shown in Fig. 6 is 3.28×10^5 cm^{-2}.

4. Application of the FAOM for scanning of large samples

Fig. 7 illustrates track density distributions that are obtained using the FAOM. Fig. 7(a) and (b) shows the track density distributions in CR39 and LR-115 2B detectors that were exposed to weakly moderated spallation neutrons in the interaction

of 1 GeV protons with extended cylindrical lead target (see [6,7] for details of the experimental set-up). In the case of the LR-115 detector tracks are mainly due to the $^{10}B(n, \alpha)^7$ Li reactions while in the case of the CR39 majority of the tracks are due to neutron induced recoils in the constituent nuclei of the detector material (i.e. H, C and O). Obviously the track density distributions in LR-115 and CR39 detectors illustrate the spatial distributions of the thermal and fast neutrons respectively in the experimental set-up.

Both detectors have a length of 31 cm and width of ∼1.5 cm. In both types of the detectors an area of 0.5×31 cm^2 was scanned using the computer controlled moving stage of the FAOM. Every experimental data point in Fig. 7 represents the average track density calculated from 125 fields of view, each covering an area of ∼0.2×0.2 mm^2 on the detector surface. All together in a given sample 38,500 fields of view were scanned at a rate of ∼1 s per field of view. The most time consuming parts of the scanning process are the actual mechanical movement of the stage followed by the auto-focusing. A comparison of the observed track densities with those obtained from Monte-Carlo simulations [7] shows that deviations between the experimental and simulated track densities are caused mainly by other parameters in the experiment rather than the counting inaccuracy of the FAOM.

Obviously for high track densities ($\geqslant 5 \times 10^5$ cm^{-2}) and/or highly over etched samples, the overlapped tracks will be too many and FAOM will under estimate the track density. Such an underestimations are the consequences of the geometrical restrictions imposed on the track recognition as well as due to the loss of the contrast between the tracks and background. In such circumstances a calibration curve that relates the FAOM counts to the true counts (obtained say by manual counting) must be used to apply appropriate corrections to the counts obtained by the FAOM.

We have also found the FAOM a useful tool for examining the cleanliness and integrity of the electronics of silicon strip detector modules (overall size of ∼12×7 cm^2) that will be used in the ATLAS detector [8].
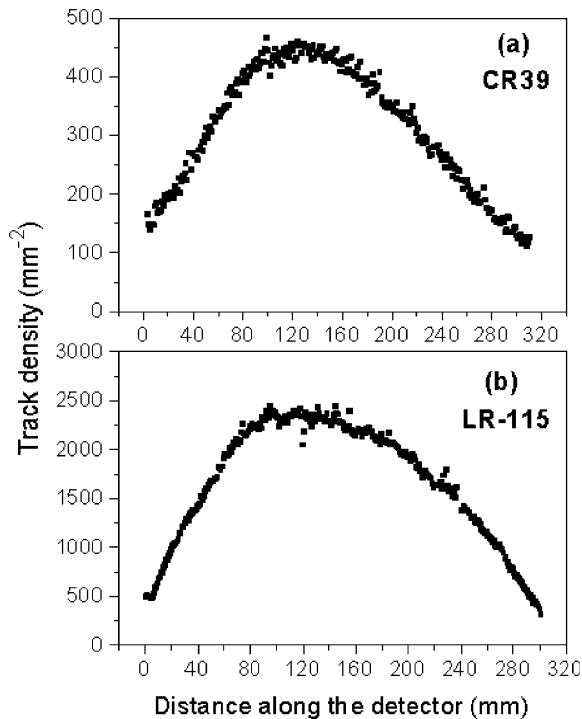

Fig. 7. Track density distributions in CR39 and LR-115 2B plastic track recorders, which were obtained using the FAOM. In LR-115 detector tracks are mainly due to the $^{10}B(n, \alpha)^7$ Li reactions while in the case of the CR39 majority of the tracks are due to neutron induced recoils in the constituent nuclei of the detector material (i.e. H, C and O). Both detectors have a length of 31 cm and width of ∼1.5 cm. In both types of the detectors an area of 0.5×31 cm^2 was scanned. Every experimental data point represents the average track density calculated from 125 fields of view, each covering an area of ∼0.2×0.2 mm^2 on the detector surface. For a given detector 38,500 fields of view were scanned at a rate of ∼1 s per field of view.

5. Discussion and conclusions

The FAOM described in the present paper has been tested in analysis of the particle tracks in LR-115 and CR39 track detectors. The existing form of the FAOM allows one to measure the density of micro-objects in the sample, to determine the area of each object and optically slice the object of interest. With some extension of the code, the latter capability may be used to produce a 3D profile of the object. In the case of particle tracks, such an object profile determination could be used for identification of the individual particles responsible for formation of the tracks. Such an application will be possible only if production of a large number of distinctly different images of the object, each representing a different focal plane, is possible. This by itself will depend on the track length, the incidence angle of the particle and magnification of the objective used in the analysis (also it is expected that the illumination method of the specimen will plays a significant role).

The FAOM system (hardware and software) presented in this paper is fast enough to allow scanning of the macro-samples on a reasonable time scale. For example, in the case of track counting ~1 s per field of view (frame) was achieved.

The information provided in this paper on the hardware and software of the FAOM can act as a foundation for further extension and improvement of the system to suit the requirements of the interested laboratories. The relevant techniques and methods described in the literature by other authors, such as those in [3] can be implemented in the FAOM with relative ease.

References

[1] W. Trakowski, B. Schöfer, J. Dreute, S. Sonntag, C. Brechtmann, J. Beer, H. Drechsel, W. Heinrich, Nucl. Instr. and Meth. A 225 (1984) 92.
[2] P.B. Price, W. Krischer, Nucl. Instr. and Meth. A 234 (1985) 158.
[3] A.P. Fews, Nucl. Instr. and Meth. B 72 (1992) 91.
[4] A. Boukhair, A. Haessler, J.C. Adloff, A. Nourreddine, Nucl. Instr. and Meth. B 160 (2000) 550.
[5] S.R. Hashemi-Nezhad, M. Dolleiser, Radiat. Meas. 28 (1997) 839.
[6] S.R. Hashemi-Nezhad, R. Brandt, W. Westmeier, H. Westmeier, J.-S. Wan, P. Vater, Radiat. Meas. 34 (2001) 319.
[7] S.R. Hashemi-Nezhad, M. Dolleiser, R. Brandt, W. Westmeier, R. Odoj, M.I. Krivopustov, B.A. Kulakov, A.N. Sosnin, Nucl. Instr. and Meth. A 493 (2002) 121.
[8] ATLAS Collaboration, ATLAS inner detector technical design report, CERN/LHCC/97-17.